Regulation of adhesion behavior of murine macrophage using supported lipid membranes displaying tunable mannose domains

T Kaindl[1], J Oelke[1,2], A Pasc[3], S Kaufmann[1], O V Konovalov[4], S S Funari[5], U Engel[6], A Wixforth[2] and M Tanaka[1]

[1] Physical Chemistry of Biosystems, Institute of Physical Chemistry, University of Heidelberg, Heidelberg D-69120, Germany
[2] Department of Physics, University of Augsburg, Augsburg D-86159, Germany
[3] LERMAB—EA 4370, Université Henri Poincaré Nancy 1, BP 70239, Vandoeuvre-lès-Nancy F-54506, France
[4] European Synchrotron Radiation Facility (ESRF), Grenoble Cedex 9 38053, France
[5] Hamburger Synchrotronstrahlungslabor at DESY, Hamburg D-22603, Germany
[6] Nikon Imaging Center at the University Heidelberg, BIOQUANT, Heidelberg D-69120, Germany

E-mail: tanaka@uni-heidelberg.de

Abstract

Highly uniform, strongly correlated domains of synthetically designed lipids can be incorporated into supported lipid membranes. The systematic characterization of membranes displaying a variety of domains revealed that the equilibrium size of domains significantly depends on the length of fluorocarbon chains, which can be quantitatively interpreted within the framework of an equivalent dipole model. A mono-dispersive, narrow size distribution of the domains enables us to treat the inter-domain correlations as two-dimensional colloidal crystallization and calculate the potentials of mean force. The obtained results demonstrated that both size and inter-domain correlation can precisely be controlled by the molecular structures. By coupling α-D-mannose to lipid head groups, we studied the adhesion behavior of the murine macrophage (J774A.1) on supported membranes. Specific adhesion and spreading of macrophages showed a clear dependence on the density of functional lipids. The obtained results suggest that such synthetic lipid domains can be used as a defined platform to study how cells sense the size and distribution of functional molecules during adhesion and spreading.

(Some figures in this article are in colour only in the electronic version)

1. Introduction

Plasma membranes in nature are known to have intrinsically asymmetric compositions of lipids in their cytoplasmic and extracellular leaflets [32]. They are postulated to form laterally organized functional domains enriched with sphingolipids, cholesterol, and phospholipids [22, 36, 37], often called 'rafts', which play key roles in complex cellular functions, such as endocytic traffic, signal transduction, and cell adhesion [3, 8, 15, 18, 24, 36]. The spatial confinement of ligand molecules would allow for the fine-adjustment of binding strength via cooperative, polyvalent interactions between proteins and ligand molecules, such as carbohydrate–protein interactions [26, 31, 40, 42]. For example, the binding affinity of synthetic sialyl Lewis^X tetrasaccharide (sLe^X, Neu5Acα2-3Galβ1-4(Fucα1-3)GlcNAc) molecules and selectin receptors (K_d = 0.1–5 mM) [9, 17, 21] in solution is by three to four orders of magnitudes weaker than

the corresponding value reported by *in vivo* assays (K_d < 1 μM) [17, 39].

Many recent studies demonstrated that raft-like domains could be formed in artificial membrane systems (Langmuir monolayers and giant lipid vesicles) composed of synthetic 'raft mixtures' [2, 11, 12, 23], suggesting that self-assembling of lipids predominantly contributes to the formation of micro-domains. However, despite intensive studies in these years, domains composed of complex lipid mixtures are found to be either highly polydispersive, or coalesce into large domains. Thus, such inhomogeneous domains, whose diameters are often comparable to those of cells, cannot be used as well defined sub-cellular structures to regulate cell behaviors. In our previous account [17], we designed synthetic lipids with sLe^X head groups and semi-fluorinated lipid anchors, which formed micro-domains in phospholipid membranes. Although we demonstrated that these synthetic domains can be utilized to regulate the adhesion of Chinese hamster ovarial cells expressing E-selectin, we found that a higher degree of fluorination is necessary to form highly ordered micro-domains. Recently, we synthesized lipids with perfluorinated anchors (chain length, $n = 17$), and reported that they adopt a crystalline, helical conformation and formed highly uniform, strongly correlated domains [29]. The domain size ($L = 350$ nm) close to the optical resolution can be quantitatively determined by grazing-incidence x-ray diffraction with analyzer crystal optics. The interactions between these nano-domains turned out to be highly repulsive: the long-range ordering can reach up to a distance eight times larger than the domain size, which can be interpreted within the theoretical framework of two-dimensional colloidal crystallization.

In this work, we synthesized two new perfluorinated lipids ($n = 10$ and 13), and found a significant impact of the fluorocarbon chain length on the domain size and the inter-domain interaction. Based on the full characterization of the membranes by a combination of various surface sensitive techniques, we were able to quantitatively calculate the minimal free energy and, thus, the equilibrium domain size within the framework of an effective dipole potential model. An excellent agreement between experimental results and theoretical calculation strongly suggested the rational design of tailored micro- and nano-domains of perfluorinated lipids displaying biofunctional groups.

As the first step, we functionalized one of the lipids ($n = 10$) with mannose, and utilized the micro-domains to regulate the cell adhesion behavior. In nature, mannose is recognized by the mannose receptor (MR), which is a 180 kDa C-type lectin with multiple carbohydrate recognition units, playing important roles in internalization of various sugar-containing proteins [13, 14, 34]. In this study, we chose the murine macrophage cell J774.A1 as a cell type; it expresses MR at a surface concentration of around 46.000/cell ($K_d \sim$ 92.9 nM) [16]. In this study, we highlighted changes in cell shapes and cytoskeleton remodeling caused by the density of mannose-functionalized domains.

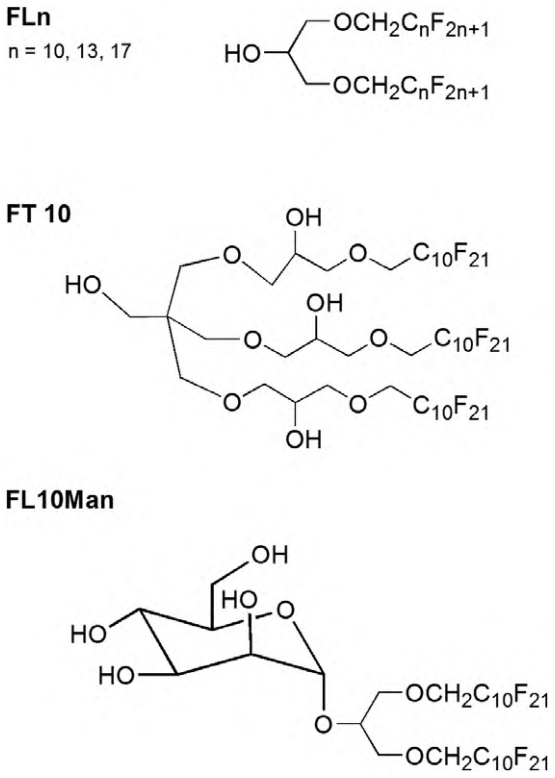

Scheme 1. Chemical structure of synthetic fluorinated lipids used in this study.

2. Materials and methods

2.1. Fluorinated amphiphilic molecules

1,2-dioleoyl-*sn*-glycero-3-phosphocholine (DOPC) was purchased from Avanti Polar Lipids Inc. (Alabaster, AL-USA), and 1,2-dihexa-decanoyl-*sn*-glycero-3-phosphoethanolamine, triethylammonium salt (TexasRed-DHPE) from Invitrogen (Karlsruhe, Germany). The fluorocarbon chains **FLn** ($n = 10$, 13, 17) of the anchor lipids were connected to glycerol backbones. To study the influence of the number of fluorocarbon chains, a lipid with three fluorocarbon chains (**FT10**) was synthesized. In the last step, the hydroxy-headgroup was replaced by a α-D-mannose monomer for **FL10Man** molecules to highlight the impact of carbohydrate ligands on cell adhesion behavior. The synthesis of fluorinated lipid molecules followed the previously reported synthetic pathway [20, 28, 29], whose chemical structures are shown in scheme 1. The detailed information on the synthesis is reported in appendix A.

2.2. Cell culture

The murine macrophage cell line J774A.1 expressing the mannose binding receptor was purchased from DSMZ GmbH (Braunschweig, Germany) and maintained in 89% Dulbecco's MEM, 10% fetal bovine serum (FBS) and 1% penicillin and streptomycin (Sigma-Aldrich Chemie GmbH, Munich, Germany). Before harvesting the cells with a scraper, they were kept for at least 16 h (corresponding to half of the cell division cycle) in FBS and glucose-free medium for

synchronization. Cell adhesion experiments were carried out in 140 mM NaCl and 1 mM CaCl buffered with 10 mM TRIS (pH 7.4).

2.3. Sample preparation

Prior to the monolayer deposition, cleaned glass slides were hydrophobized with octadecyltrimethoxysilane (ABCR GmbH, Karlsruhe, Germany) [19]. The lipid mixtures were dissolved in 1:1 (v/v) 1,1,2-trichlorotrifluorethane (Riedel-de Haën, Seelze, Germany): chloroform solution at a concentration of 0.8 mM. For the visualization of domains, 0.1 mol% of TexasRed-DHPE was doped into the stock solution. The stock solution was spread onto a water subphase of a Langmuir film balance (Nima Technology Ltd, Coventry, UK). After evaporation of the solvents, the film was compressed at a low speed (0.01 $Å^2$ $molecule^{-1}$ s^{-1}) to a surface pressure of $\pi = 20$ mN m^{-1} at $T = 293$ K. After the transfer onto a hydrophobic glass slide by horizontal Langmuir–Schaefer transfer, the sample was kept under water and assembled with a μ-Slide I flow chamber lid (Ibidi GmbH, Martinsried, Germany). For the analysis of cell shapes, the cells were fixed overnight in 3.7 vol% paraformaldehyde at 4 °C and made permeable with 0.2 vol% TritonX-100 before staining with Alexa Fluor488 phalloidin (Invitrogen GmbH, Karlsruhe, Germany). All the other chemicals were purchased from Sigma-Aldrich Chemie GmbH (Munich, Germany) and used without further purification. Throughout the study, double de-ionized water with a specific resistance of $R > 18$ MΩ cm^{-1} (TKA GmbH, Niederelbert, Germany) was used.

2.4. Microscopy

Fluorescence microscopy and microinterferometry (Reflection Interference Contrast Microscopy, RICM) were carried out on an Axiovert 200 inverted microscope (Carl Zeiss, Göttingen, Germany) equipped with an Orca ER CCD camera (Hamamatsu Photonics, Herrsching, Germany). Since all fluorescent lipid tracers are excluded from the fluorinated domains into the fluid lipid matrix [29], **FLn** domains appeared as dark spots that were identified below the threshold intensity using Cellenger software (Definiens AG, Munich, Germany). To average on local sample variations, at least 2000 domains on more than 50 different regions were evaluated. RICM was performed at a wavelength of 546 nm using a PlanNeofluar 63×/1.25 Antiflex objective. Cell culture conditions were maintained by means of a HT200 thermostated chamber (Ibidi GmbH, Martinsried, Germany) flushed width 5% CO_2.

Image stacks were recorded with 200 nm z-spacing on a Perkin Elmer Ultraview spinning disc confocal setup mounted on a inverted microscope equipped with a 60× Plan Apo VC water immersion objective, NA 1.2 (Nikon, Düsseldorf, Germany). Before applying image stacks to the rendering process, the images were deconvolved with Huygens software 3.4 from Scientific Volume Imaging (Hilversum, The Netherlands).

2.5. X-ray scattering

Grazing-incidence x-ray diffraction (GIXD) measurements were carried out at the ID 10B beam line at the European Synchrotron Radiation Facility (ESRF, Grenoble, France). A monochromatic synchrotron x-ray beam ($\lambda = 1.5$ Å) impinges on to the monolayer interface at a grazing angle ($\alpha_i = 0.8\alpha_c$) below the critical angle (α_c) of total reflection. The intensity of the diffracted beam was detected with a linear position sensitive detector mounted in vertical direction. The horizontal scattering vector component q_{xy} was measured as a function of the azimuthal scattering angle Ψ. Small angle x-ray scattering (SAXS) experiments were carried out at the beam line A2 at the Hamburger Synchrotronstrahlungslabor (HASYLAB, Hamburg, Germany). The lipid mixtures were filled in quartz capillaries with an inner diameter of 1 mm (Hilgenberg, Malsfeld, Germany), briefly centrifuged, and flame-sealed.

3. Theory of finite domain size

To understand the influence of fluorocarbon chain lengths on the size of domains, we used a steady state model to describe the free energy F of a binary lipid mixture. According to the equivalent dipole model [27], the free energy F of domains with a finite size R can be written as the sum of the electrostatic energy F_{el} and the tension energy F_λ: $F = F_{el} + F_\lambda$. The electrostatic free energy F_{el} is expressed by

$$F_{el} = 2\pi R(\Delta m)^2 \ln\left(\frac{e^2\delta}{4R}\right), \tag{1}$$

where Δm is the difference in the molecular dipole densities between fluorinated lipid domain and phospholipid matrices, δ is the dipole–dipole distance at the phase boundary, and e is Euler's constant. The tension energy is written as:

$$F_\lambda = 2\pi R\lambda, \tag{2}$$

where $\lambda = \Delta\gamma \times l_{FL} + \gamma \times \Delta l$.

The line tension λ is separated into two terms, where γ is the surface tension at fluorocarbon–air interface, $\gamma_{CF-air} = 9.5$ mN m^{-1} [7], and l_{CF} is the molecular length of fluorinated lipids. Δl and $\Delta\gamma$ reflect the mismatch in the molecular length and the difference in the surface tensions γ_{CH-air}–$\gamma_{CF-air} = 9.8$ mN m^{-1} [7]. l_{FL} is the length of the fluorinated lipid molecule, while Δl the mismatch in molecular lengths between phospholipids and fluorinated lipids. At equilibrium, the minimization of the free energy F, yields the equilibrium radius R_{eq} of the domain size:

$$R_{eq} = \left(\frac{e^3\delta_{chain}}{4}\right)\exp\left(\frac{\lambda}{\Delta m^2}\right). \tag{3}$$

This means, once the four structural parameters, Δm, δ_{chain}, l_{FL}, and Δl, are determined experimentally, one can calculate the equilibrium domain size. In the following section, we present the structural parameters extracted from the experiments; these will be introduced into the model and compared with the theoretical prediction.

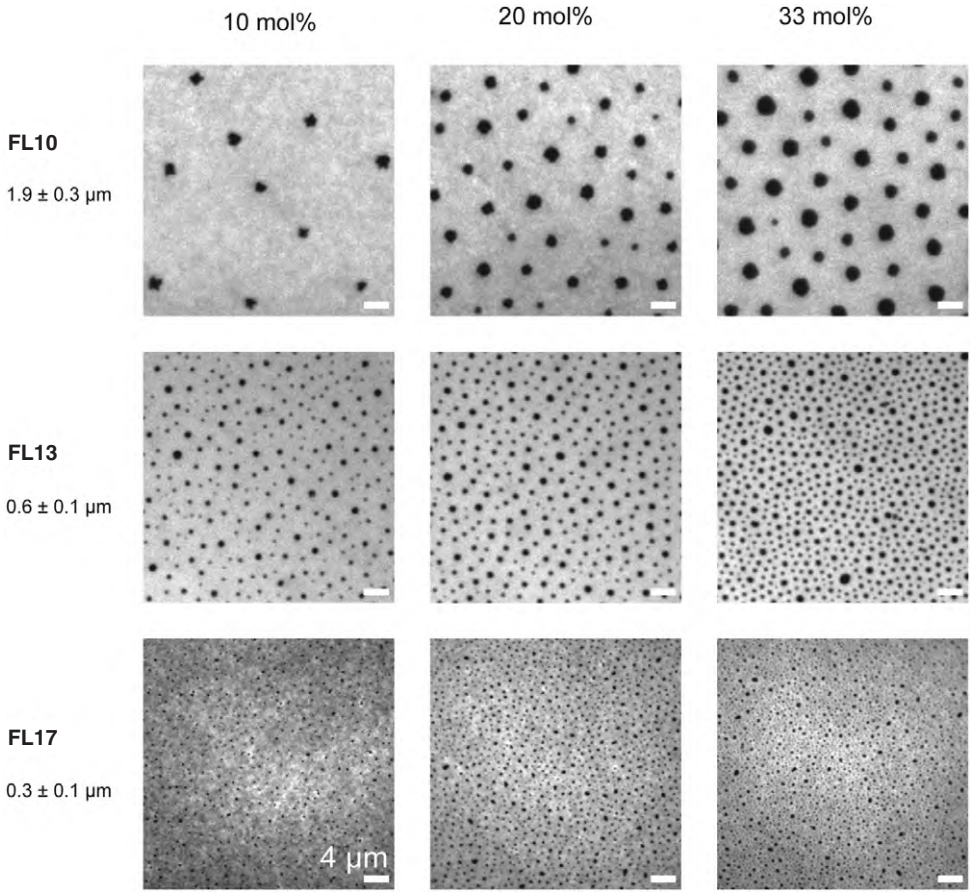

Figure 1. Fluorescence images of 10, 20, and 33 mol% mixtures of **FL10** (upper row), **FL13** (middle row), and **FL17** (lower row) show the de-mixing of fluorinated molecules into circular domains (black dots) with narrow size distribution in a phospholipid matrix (bright background). All scale bars are 4 μm.

4. Results and discussion

4.1. Influence of fluorocarbon chain length on the domain size

Figure 1 represents the fluorescence images of the phospholipid (DOPC) monolayers doped with **FL10** (top row), **FL13** (middle row), and **FL17** molecules (bottom row). As shown in the figure, **FLn** lipids form circular domains, and the size of domains seems to depend on the length of fluorocarbon chains but not on the molar fraction of **FLn** lipids: the average diameters of fluorinated lipid domains $\langle d_{\rm exp}\rangle$ are 1.9 ± 0.3 μm for **FL10**, 0.6 ± 0.1 μm for **FL13**, and 0.3 ± 0.1 μm for **FL17**, respectively[7]. The size of **FL17** domains estimated from the image analysis (0.3 ± 0.1 μm) seems to be in reasonable agreement with that calculated from the peak width, $d_{\rm GIXD} = 0.35$ μm.

Since the clear dependence of domain size on the molecular length that we observed here seems to agree well with the theoretical prediction within the framework of the equivalent dipole model, we determined the four structural parameters required for the calculation of the equilibrium domain size. First, the chain–chain distance in **FLn** domains could be determined from the GIXD experiments. All fluorinated lipids show a single Bragg peak at $q_z = 0$ Å^{-1}, suggesting that fluorocarbon chains are arranged in a hexagonal lattice and take an upright conformation with no detectable molecular tilt. From the position of the Bragg peaks, $q_{xy} = 1.27 \pm 0.01$ Å^{-1} for **FL10**, 1.28 ± 0.01 Å^{-1} for **FL13**, and 1.28 ± 0.01 Å^{-1} for **FL17**, it is possible to calculate the inter-chain distance of 5.73 ± 0.01 Å for **FL10**, 5.67 ± 0.01 Å for **FL13**, and 5.65 ± 0.01 Å for **FL17**, respectively. These values agree well with the value reported from the crystallography of ordered fluorocarbon chains taking a helical conformation, 5.54 Å [6]. Therefore, taking the average distance between the hydrocarbon chains of DOPC in a fluid state (6.5 Å, calculated from the pressure–area isotherm of a pure DOPC monolayer), the dipole–dipole distance at the phase boundary, $\delta \sim 6.1$ Å, could be obtained. In the next step, we determined the length of **FLn** molecules $l_{\rm FL}$ by SAXS measurements of **FLn** suspensions (appendix B). The obtained SAXS patterns were fitted with a three slab model (water, lipid head groups, fluorocarbon chains) to reconstruct the electron density profiles, yielding the molecular lengths of $l_{\rm FL10} = 12.8 \pm 0.5$ Å, $l_{\rm FL13} = 16.8 \pm 0.5$ Å, and $l_{\rm FL17} = 21.9 \pm 0.5$ Å. From the molecular height of DOPC $l_{\rm DOPC} = 18.5 \pm 0.5$ Å [38] and the length mismatch Δl can be calculated for all the **FLn**

[7] Since the determination of the size of FL17 domains from a pixel analysis might be erroneous, we carried out GIXD of the FL17 monolayer with a Si(111) analyzer crystal optics [25].

Table 1. Summary of the structure parameters (l_{FL}, q_{xy}, δ) used for the calculation of the equilibrium diameter D_{eq} of each **FLn** lipid. The position of the first minimum of the potential of mean force r_{PMF} and its apparent spring constant k' corresponding to [**FLn**] = 33 mol% are presented in the table.

	FL10	**FL13**	**FL17**
$\langle d_{exp} \rangle$ (μm)	1.9 ± 0.3	0.6 ± 0.1	0.3 ± 0.1
q_{xy} (Å^{-1})	1.27 ± 0.01	1.28 ± 0.01	1.28 ± 0.01
δ_{FLn} (Å)	5.73 ± 0.01	5.67 ± 0.01	5.65 ± 0.01
l_{FL} (Å)	12.8 ± 0.5	16.8 ± 0.5	21.9 ± 0.5
D_{eq} (μm)	2.2 ± 0.3	0.8 ± 0.1	0.25 ± 0.03
r_{FLn} (μm)	6.5 ± 1.3	1.7 ± 0.5	0.8 ± 0.2
k' (μm^{-2})	0.48 ± 0.01	3.1 ± 0.1	6.5 ± 0.7

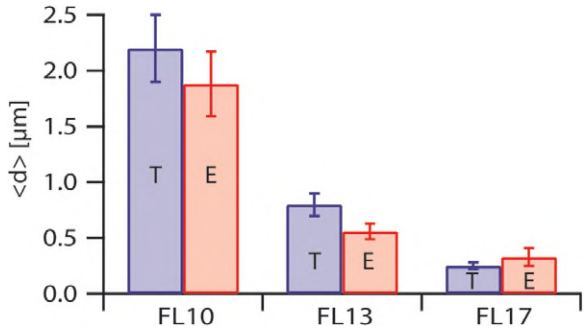

Figure 2. Comparison of mean diameter $\langle d \rangle$ between experimental (E) and theoretical (T) values calculated from equivalent dipole model.

molecules. The summary of all the structural parameters is presented in table 1.

The other parameter, the molecular dipole difference Δm, can be measured using a film balance equipped with a vibrating plate electrode (Kibron, Espoo, Finland). The dipole potentials of pure **FLn** monolayers at $\pi = 20$ mN m^{-1} were found to be almost independent of the chain length, (−630 mV). The negative dipole moment projected to the direction normal to the surface is dominated by the electron-accepting CF_3-terminal group [35]. Therefore, Δm is mainly influenced by the intermolecular distance or density of the molecules. This finding seems consistent with GIXD results that indicate that all **FLn** molecules have an upright conformation, having a finite inter-chain distance of ∼5.7 Å that remains unchanged for different surface pressures (data not shown). In fact, a DOPC monolayer has a dipole potential of an opposite sign (+315 mV) due to its electron-donating CH_3-terminal group [4]. The measured dipole potential V_{dip} can be written as a function of the dipole density m (and thus the molecular dipole moment μ, by taking the area per molecule A into consideration) by using the Helmholtz equation:

$$V_{dip} = \frac{m}{\varepsilon_0 \varepsilon_r} = \frac{\mu}{\varepsilon_0 \varepsilon_r A}, \tag{4}$$

where ε_0 is the permittivity of free space, and ε_r is the dielectric constant of the monolayer. In order to calculate the equilibrium radius domain size R_{eq}, the dielectric constant ε_r is the only remaining unknown parameter. In fact, as is obvious from equations (3), and (4), the choice of the dielectric constant ε_r is critical, due to the exponential dependence on ε_r^2. The value significantly depends on the location of the molecules at the interface between air ($\varepsilon_{air} = 1$) and water ($\varepsilon_{water} = 78$), which is, in a realistic viewpoint, difficult to define. Therefore, starting from the dielectric constant of fluorinated liquid medium $\varepsilon_{F,liquid} \sim 5$, we took arbitrary ε_r values and calculated the equilibrium domain diameter, $D_{eq} = 2 \times R_{eq}$, for **FL10**, **FL13**, and **FL17** in order to achieve an agreement with three experimental values $\langle d \rangle$. The optimal agreement is obtained if one takes $\varepsilon_r = 6$, where the theoretically calculated values fall within the experimental errors (figure 2). In a recent account [5], the molecular dipole moment of alcohols with single fluorocarbon chains in vacuum were calculated to be $\mu = 2.8$ D. If one assumes that the dipole moment of the **FLn** lipids with two chains is 5.6 D, an apparent dielectric constant of $\varepsilon_r = 5.5$ can be obtained, showing reasonable agreement with the optimal value we obtained in a self-consistent manner ($\varepsilon_r = 6$).

Previously, Lipowsky and Dimova [25] proposed a relatively simple approach to describe the line tension λ of the domain boundary in binary lipid mixtures using the size of lipid molecules L and the energy difference ΔU between the lipids in domains (A) and matrix lipids (B):

$$\lambda = \frac{\Delta U}{L} = \frac{1}{L}\left[\frac{1}{2}(U_{AA} + U_{BB}) - U_{AB}\right]. \tag{5}$$

Here, U_{AA} and U_{BB} represent the homo-pair interactions, while U_{AB} is the hetero-pair interaction at the domain boundary. The uniqueness of our experimental system is that the contribution from heterotypic interactions between fluorocarbon chains and hydrocarbon chains U_{AB} is negligibly small [10, 33]. Since the homophilic interactions between matrix lipids (U_{BB}) are constant, the dominant parameter that determines the line tension in this model is the homophilic interactions between fluorocarbon chains U_{AA}. However, since U_{AA} is proportional to the length of fluorocarbon chains, the elongation of fluorocarbon chains should lead to an increase in λ, resulting in an increase in the equilibrium domain radius R_{eq}. This is contradictory to the tendency that we found experimentally, suggesting that the influence of the pair potential considered in equation (5) is not sufficient to calculate R_{eq}. Here, the mismatch in the molecular length (ΔL in equation (2)) should additionally be taken into consideration. Thus, in this study, we used equation (3) to calculate the R_{eq} values.

4.2. Correlation between synthetic lipid domains

The strength of inter-domain correlations was quantitatively evaluated by calculating the radial distribution function $g(r) = [dN(r + dr)/d(A + dA)] \times N/A$ for >2000 domains [30]. Within the framework of the inverse work theorem, $g(r)$ can be related to so-called potential of mean force—$w(r)$:

$$-\frac{w(r)}{k_B T} \propto \ln[g(r)]. \tag{6}$$

The potentials of mean force calculated for [**FLn**] = 33 mol% are presented in figure 3. Note that the distance r is

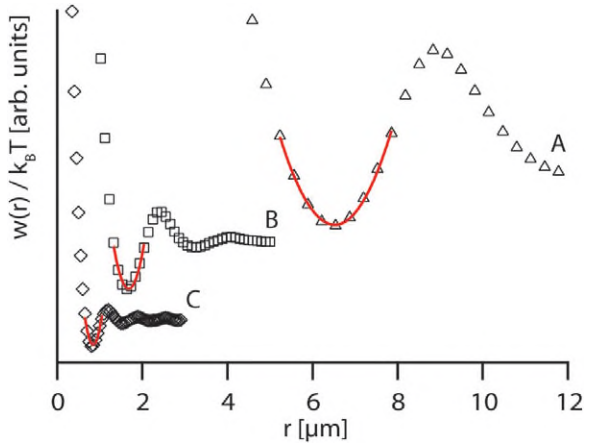

Figure 3. Potentials of mean force $w(r)/k_BT$ calculated for 33 mol% of (A) **FL10**, (B) **FL13**, and (C) **FL17** in DOPC. As indicated by the red lines, the potential in the vicinity of the first minima can be well approximated as harmonic.

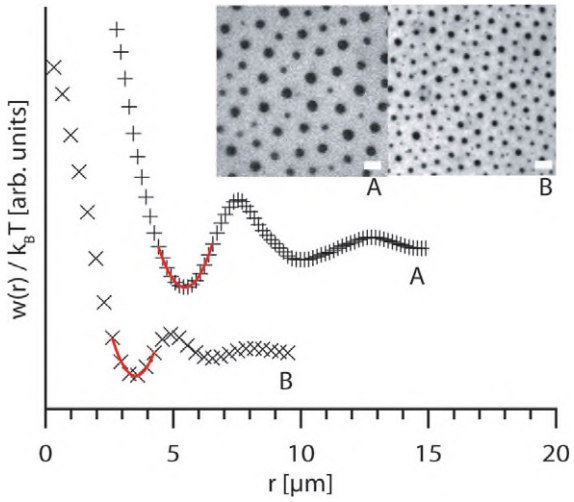

Figure 4. Potentials of mean force (main panel) calculated from the fluorescence images (inset) of 33 mol% domains of (A) **FT10** and (B) **FL10Man**.

not normalized by the domain size in the figure to highlight the impact of the molecular structures on the interaction potentials. As presented in the figure, the distance to the first order minimum monotonically increases from $r_{FL17} = 0.8 \pm 0.2\ \mu$m, $r_{FL13} = 1.7 \pm 0.5\ \mu$m to $r_{FL10} = 6.5 \pm 1.3\ \mu$m according to the decrease in the fluorocarbon chain length. Moreover, the potentials near the first order minima are well approximated as harmonic (red lines in figure 3), yielding the spring constants of $k'_{FL17} = 6.5 \pm 0.7\ \mu\text{m}^{-2}$, $k'_{FL13} = 3.1 \pm 0.1\ \mu\text{m}^{-2}$, and $k'_{FL10} = 0.48 \pm 0.01\ \mu\text{m}^{-2}$, respectively. The observed tendency suggests that the confinement of **FLn** domains is shallower according to the decrease in the fluorocarbon chain length. It should be noted that this potential, obvious from its definition, is of free energy nature and includes many body interactions, where the long-range correlations can readily reach up to a distance that is several times larger than the domain size. Here, $w(r)$ can be equivalent to the direct pair potentials between two particles only for highly diluted system. In fact, uncorrelated interactions following the Yukawa potential [41] can be observed at [**FLn**] < 5 mol% (appendix C).

4.3. Influence of molecular structures

To further examine the impact of molecular structures on the size and correlation of fluorinated lipid domains, we also investigated the influence of the number of fluorocarbon chains. For this purpose, we prepared monolayers doped with **FT10**, which has three fluorocarbon chains. Figure 4(A) represents the potential of mean force calculated for **FT10** domains (33 mol%) and the corresponding fluorescence image. It is notable that the average domain size $\langle d_{exp} \rangle = 1.7 \pm 0.3\ \mu$m and the position of the first potential minimum $r_{FT10} = 5.5 \pm 0.8\ \mu$m are comparable to those of **FL10** (table 1). This finding seems fully consistent with the equivalent dipole model: SAXS proves that the length of **FT10** is almost identical to that of **FL10**, and GIXD indicates that fluorocarbon chains of **FT10** take an upright orientation, keeping the same inter-chain distance.

In order to utilize such strongly correlated, fine-adjustable lipid domains to regulate the cell adhesion behavior, we coupled a simple monosaccharide, α-D-mannose, to the **FL10** head group (**FL10Man**). In contrast to the results obtained for **FT10**, **FL10Man** exhibited a slight but distinct change in both size and correlation (figure 4(B)). Both the domain size ($\langle d_{exp} \rangle = 1.2 \pm 0.2\ \mu$m) and the position of the first minimum ($r_{FL10Man} = 3.6 \pm 1.7\ \mu$m) were smaller than those of **FL10**, suggesting a decrease in the repulsive interactions between domains. In fact, the harmonic potential assumed near the first minimum became sharper, which can be characterized by a larger spring constant. Although we observed no changes in the molecular length or orientation within our experimental resolution, the obtained results suggest the slight influence of saccharide head groups on the size and correlation of the fluorinated lipid domains.

4.4. Adhesion of murine macrophage on FL10Man domains

The three-dimensional shapes of J774A.1 cells reconstructed from confocal microscopy images (upper row) and the microinterferograms of live cells taken under the same conditions (bottom row) are presented in figure 5. Here, murine macrophage cells were incubated on supported membranes consisting of (a) pure phospholipids (DOPC), (b) 33 mol% **FL10Man** and 67 mol% DOPC, and (c) pure **FL10Man** for 2 h. It should be noted that the density of cells found on DOPC membranes (figure 5(a)) is very small in comparison to those on membranes with **FL10Man** (figures 5(b) and (c)). In fact, more than 90% of cells found on the surface could be removed by a gentle exchange of the culture medium, indicating that the adhesion on phospholipid membranes is weak and non-specific. The fluorescence image with phalloidin labeling (figure 5(a), top) implies that most cells are round, and no spreading of the peripheral membrane could be observed. In fact, the contact area of cells could hardly be identified with RICM ($A_{contact} < 10\ \mu\text{m}^2$) due to a significant height fluctuation of cells near the surface (figure 5(a), bottom).

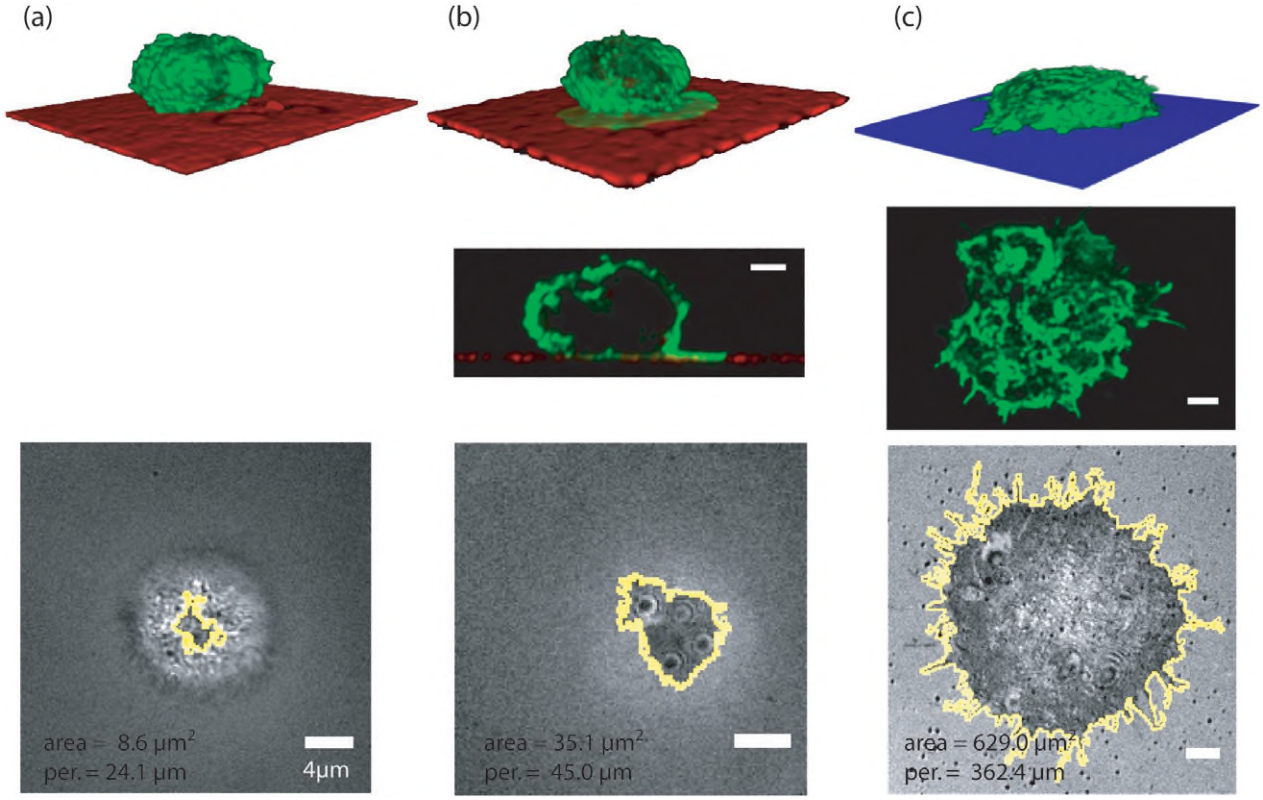

Figure 5. J774A.1 cells incubated for 2 h on (a) pure DOPC membranes, (b) DOPC with [**FL10Man**] = 33 mol%, and (c) pure **FL10man** membranes. The images in the upper row are three-dimensional shapes of fixed cells reconstructed from confocal microscopy images. Below, a cross sectional view of (b) and the plane of cell contact for (c) is shown. The bottom row shows microinterferograms of live cells, where the rims of the adhesion zones used for the calculation of contact areas are highlighted with yellow lines. All scale bars are 4 μm.

On the other hand, cells adherent on membranes containing **FL10Man** (figures 5(b) and (c)) could not be removed even by intensive rinsing, suggesting that the adhesion is stronger and more specific than that on pure lipid membranes. On the membrane with 33 mol% **FL10Man** ($\langle d_{\mathrm{FL10Man}} \rangle = 1.2\ \mu$m, $r_{\mathrm{FL10Man}} = 3.6\ \mu$m), a distinct spreading of the peripheral membrane could be found in the fluorescence image (figure 5(b), top and middle panel). Time lapse images of cells even suggested a stepwise spreading above the circular domains, which can be identified as round dark spots within the adhesion area (figure 5(b), bottom). Under this condition, the contact area ($A_{\mathrm{contact}} = 35\ \mu\mathrm{m}^2$), as well as the contact line perimeter ($L_{\mathrm{peri}} = 40\ \mu$m), could easily be calculated from the RICM image (figure 5(b), bottom). The cell spreading was even more prominent on pure **FL10Man** membranes, where punctate structures and filopodia near the plane of cell contact [1] can be identified (figure 5(c), top and middle panel). From the RICM image analysis, a significant increase in both the contact area ($A_{\mathrm{contact}} = 630\ \mu\mathrm{m}^2$) and the contact line perimeter ($L_{\mathrm{peri}} = 360\ \mu$m) could be observed. Further RICM studies on live cells would reveal how cells respond to the size and lateral density of functional domains during the dynamic cell spreading.

5. Conclusions

We synthesized several kinds of lipids with perfluorinated chains, and demonstrated that such synthetic (and thus non-biological) lipids can form highly uniform, strongly correlated domains in supported lipid membranes. Due to their strong oleophobic nature, all fluorinated lipids are completely demixed with matrix phospholipids, which results in a finite domain size at a wide range of mixing ratio. Full structural characterizations by the combination of x-ray scattering, surface potential measurements, and grazing-incidence x-ray diffraction revealed that the equilibrium size of domains is significantly influenced by a slight change in molecular structures. Within the framework of the equivalent dipole model, the equilibrium domain size obtained by the image analysis can be well explained in terms of the balance between the electrostatic free energy and the tension energy. Owing to a mono-dispersive, narrow size distribution of the domains, we can adopt the theory of two-dimensional colloidal crystallization to evaluate the strength of inter-domain correlations. According to the inverse work function theorem, the potentials of mean force can be deduced from the radial distribution functions of domains. The obtained results demonstrated that both the size and distribution (inter-domain correlation) can precisely be adjusted by the molecular structures of fluorinated lipids. In the last step,

we examined the potential of such synthetic lipid domains for the regulation of cell adhesion behaviors. For this purpose, we functionalized the lipid head groups with α-D-mannose, and studied the adhesion behavior of murine macrophage (J774A.1) by the combination of confocal microscopy and microinterferometry (RICM). Macrophages showed a specific adhesion and spreading on membranes containing mannose-functionalized lipids, depending on the density of functional lipids. The obtained results suggest that synthetically designed, fine-tunable domains can be used as a defined platform to study the influence of size and distribution of functional molecules on cell adhesion behaviors.

Acknowledgments

This work was financially supported by the Deutsche Forschungsgemeinschaft (Ta253/6). We thank ESRF and HASLAB for the synchrotron beam time, E Schneck for the help in experiments and data analysis, and the Nikon Imaging Center at the University of Heidelberg for imaging equipment. TK gratefully acknowledges the Heinz Götze Memorial Fellowship and JO the German Excellence Initiative via the 'Nanosystems Initiative Munich' for financial support. MT is a member of BIOQUANT. MT and UE are members of the German Excellence Cluster 'CellNetwork'.

Appendix A

The triple chain fluorinated lipid, named **FT10** was prepared by the synthetic sequence outlined below (figure A.1). In the first step, the formation of the fluorinated glycidol was performed in biphasic conditions (toluene–water) under phase-transfer catalysis. Consequently, the ring opening reaction afforded the corresponding tricatenar lipid as the major product.

A. A mixture of 1H,1H-perfluoro-1-decanol (3.7 mmol), 50% aqueous NaOH (0.84 g, 20.9 mmol, 1.7 ml H_2O), tetrabutylammonium bromide (0.079 g, 0.25 mmol), and benzene (5 ml) was stirred at room temperature for 15 min. Epichlorhydrin (2 ml, 26 mmol) was then added and the reaction mixture heated to 75 °C for 18 h. The reaction mixture was than cooled to 0 °C, filtered and washed with water. The white solid was then dried over night. Yield 89%. ^{1}H-NMR ($CDCl_3$): 2.56 (dd, 1H, CH_2 epoxide, $J = 4.6, 2.7$ Hz); 2.75 (t, 1H, CH_2 epoxide, $J = 4.6$ Hz); 3.10 (m, 1H, CH epoxide); 3.46 (dd, 1H, CH_2–O, $J = 11.8, 5.9$ Hz); 3.90 (dd, 1H, CH_2–O, $J = 11.8, 2.5$ Hz); 3.99 (t, 2H, CH_2–CF_2, $J = 13.5$).

B. In a 50 ml flask 3-hydroxy-2,2-bis(hydroxymethyl)propyl acetate (0.25 mmol) and fluorinated glycidol (0.75 mmol) were introduced. Then the air in the flask was evacuated and flooded with argon. Dichloromethane (100 ml) and five drops $BF_3{\cdot}OEt_2$ were added. The white suspension was stirred at room temperature for 12 h. Afterward five more drops $BF_3{\cdot}OEt_2$ were added and the mixture was stirred for further 12 h. Finally the solvent was evaporated and the white residue was examined by NMR-analysis (no epoxide-peaks were observed). The white residue was dispersed in methanol/dichloromethane (10 ml; 3:1 v:v) and sodium methoxide (10 mg) was added. After stirring overnight, the solution was neutralized with Amberlite IR120 (H^+), filtered and the solvent was evaporated. Yield 68%. ^{1}H-NMR ($CDCl_3$): 3.2–3.5 (20H); 3.7–3.9 (9H); elemental analysis: $C_{47}H_{33}F_{63}O_{10}$, th. %C: 28.88, %H: 1.70, exp. %C: 29.10, %H: 1.76.

The double chain fluorinated lipid, named **FLn** ($n = 10, 13, 17$) were prepared as previously described [20, 29]. **FL10Man** was synthesized by the coupling of **FL10** with the activated mannose [28] (figure A.2).

C. A solution of 1,2,3,4,6-penta-O-acetyl-D-mannopyranose (3.5 g, 9 mmol) and $NH_2NH_2{\cdot}AcOH$ (1.07 g, 1.7 mmol) in DMF (10 ml) was stirred for 10 min at 50 °C and after cooling to 20 °C, diluted with 100 ml of EtOAc. The solution was washed with water, aq. $NaHCO_3$, aq. NaCl, dried ($MgSO_4$), and evaporated *in vacuo*. Yield: 95%. ^{1}H-NMR ($CDCl_3$): 1.95, 2.01, 2.04, 2.11 ($COCH_3$); 4.03–4.07 (1H); 4.20–4.23 (2H); 5.14–5.26 (2H); 5.35 (d, 1H, Hα, β); ^{13}C-NMR ($CDCl_3$): 20.59, 20.63, 20.64, 20.79 ($COCH_3$); 62.74 (C6); 66.43, 67.96, 69,16, 70,59 (C2-5); 92.07 (C1); 169.79, 169.84, 170.05, 170.58 ($COCH_3$).

D. A solution of the oil hemiacetal (500 mg, 1.44 mmol) in dry CH_2Cl_2 (5 ml) stirred under argon, was treated successively

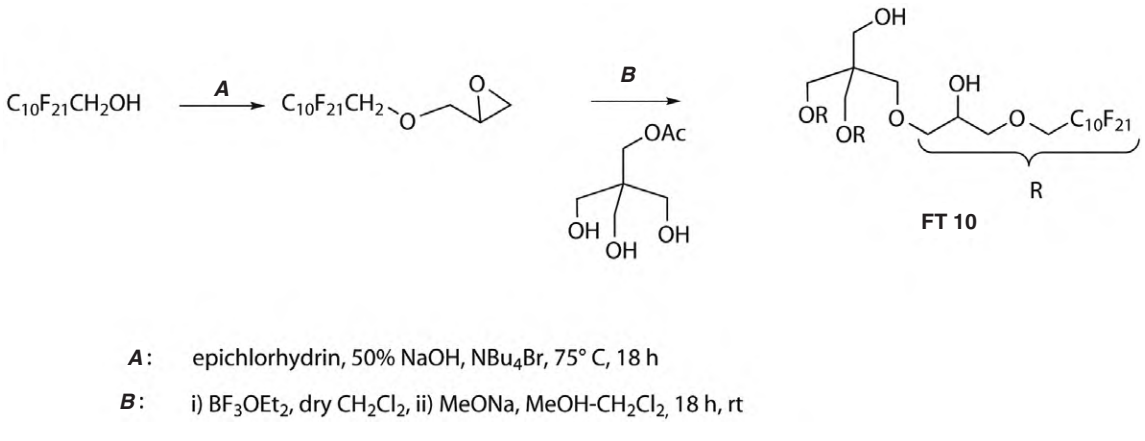

Figure A.1. Synthetic pathway of FT10.

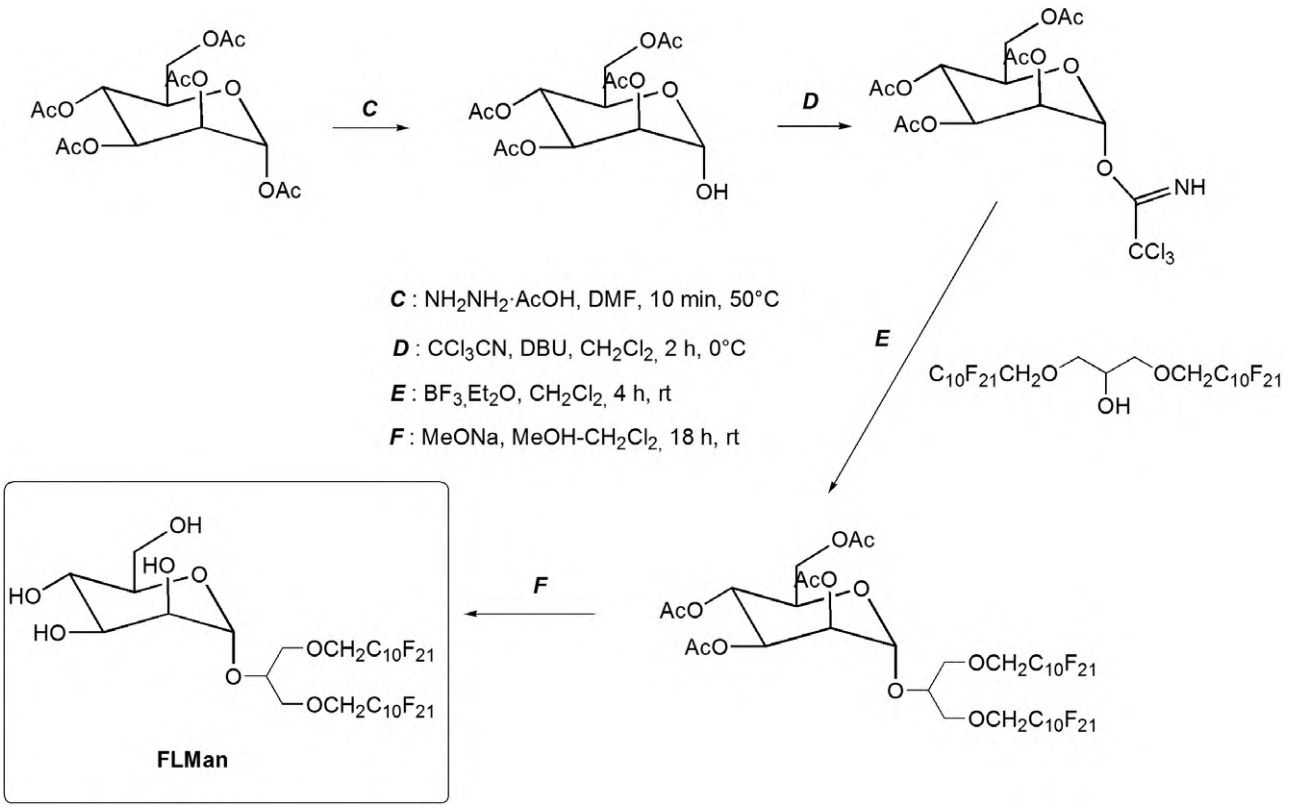

Figure A.2. Synthetic pathway of FL10Man.

with CCl_3CN (2,1 g, d = 1.44, 1.5 ml, 14.5 mmol) and 1,8-diazabicyclo[5,4,0]undec-7-ene (DBU; 22 mg, d = 1.019, 22 μl, 0.14 mmol) at 0 °C. After being stirred for 2 h at 0 °C, the mixture was directly chromatographed on SiO_2 in 1:1 hexane–EtOAc ($R_f = 0.26$). The product was isolated as a white solid. Yield 64%. ^{1}H-NMR ($CDCl_3$): 1.93, 1.96, 2.00, 2.12 ($COCH_3$); 4.05–4.25 (3H); 5.32 (2H); 5.39 (d, 1H, H2); 6.21 (d, 1H, H1); 8.81 (s, 1H, NH); ^{13}C-NMR ($CDCl_3$): 20.25, 20.41, 20.63, 20.67 ($COCH_3$); 61.75 (C6); 65.10, 67.57, 68.55, 70.96 (C2-5); 90.24 (CCl_3); 94.24 (C1); 159.33 (C=NH); 169.29, 169.36, 169.45, 170.18 ($COCH_3$).

E. To a solution of FL10 (86.5 μmol, 1 eq) and trichloroacetamidate (M = 491, 0.042 g, 86.5 μmol, 1 eq) in dry dichoromethane with molecular sieves (AW-300) was added $BF_3{\cdot}Et_2O$ (4 μl, 33 μmol, 0.3 eq) at room temperature. After 4 h the solution was neutralized with triethylamine, filtrated and evaporated under reduced pressure.

F. To a solution of fluorolipid acetylated mannose (176 μmol) in dry methanol/dichloromethane (40 ml; 3:1 v:v) was added sodium methoxide (40 mg, 0.74 mmol). After stirring overnight, the solution was neutralized with Amberlite IR120 (H^+), filtered, and absorbed on silica gel. Flash chromatography ($CHCl_3$/methanol/water 85:15:1 to 80:20:2 v/v/v) afforded **FLMan** as amorphous solid after lyophilization from water/dioxane. Yield 38%. ^{1}H-NMR (CD_3OD): 3.4–3.7 (11H); 3.84 (t, 4H); 5.21 (d, 1H); elemental analysis: $C_{31}H_{20}F_{42}O_8$, th. %C: 28.24, %H: 1.53, exp. %C: 28.62, %H: 1.58.

Appendix B

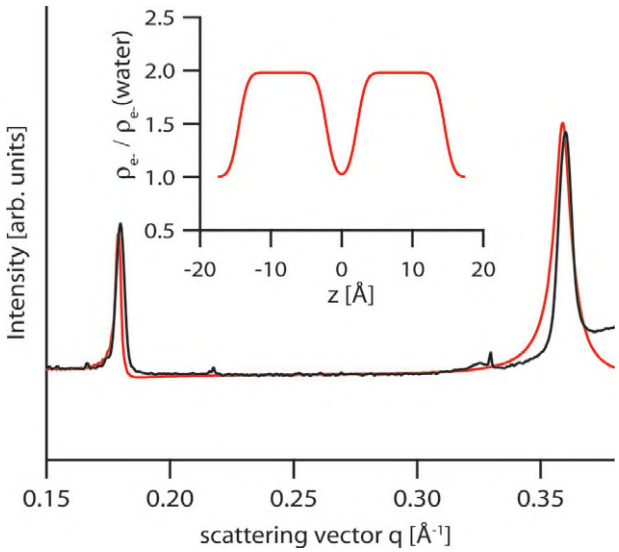

Figure B.1. SAXS intensity profile of **FL10** molecules and the best fit model (red line) used for the reconstruction of the electron density profile (inset).

Appendix C

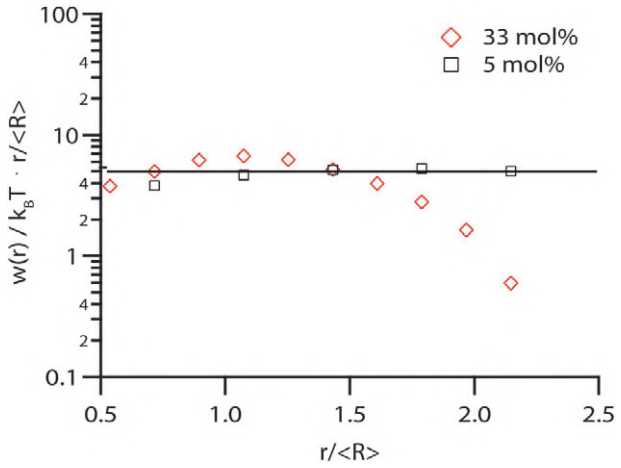

Figure C.1. Effective interactions between **FL13** nano-domains, compared to the Yukawa potential (solid line). Note that the distance r is normalized by the domain size R. Uncorrelated effective interactions that follow the Yukawa potential can be observed only at [**FL13**] 5 mol%.

References

[1] Amato P A, Unanue E R and Lansing Taylor D 1983 Distribution of actin in spreading macrophages: a comparative study on living and fixed cells *J. Cell Biol.* **96** 750–61

[2] Baumgart T, Hess S T and Webb W W 2003 Imaging coexisting fluid domains in biomembrane models coupling curvature and line tension *Nature* **425** 821–4

[3] Bovin N V 1997 *Glycoscience: Status and Perspectives* ed H-J Gabius and S Gabius (Weinheim: Chapman and Hall) p 277

[4] Brockman H 1994 Dipole potential of lipid-membranes *Chem. Phys. Lipids* **73** 57–79

[5] Broniatowski M and Dynarowicz-Latka P 2006 Semifluorinated alcohols in Langmuir monolayers—a comparative study *J. Colloid Interface Sci.* **301** 315–22

[6] Bunn C W and Howells E R 1954 Structures of molecules and crystals of fluorocarbons *Nature* **174** 549–51

[7] Chaudhury M K and Owen M J 1993 Adhesion hysteresis and friction *Langmuir* **9** 29–31

[8] Cinek T and Horejsi V 1992 The nature of large noncovalent complexes containing glycosyl-phosphatidylinositol-anchored membrane-glycoproteins and protein tyrosine kinases *J. Immunol.* **149** 2262–70

[9] Cooke R M, Hale R S, Lister S G, Shah G and Weir M P 1994 The conformation of the sialyl-Lewis-X ligand changes upon binding to E-selectin *Biochemistry* **33** 10591–6

[10] Dantzler Siebert E M and Knobler C M 1971 Interaction Virial coefficients in hydrocarbon–fluorocarbon mixtures *J. Phys. Chem.* **75** 3863–70

[11] Dietrich C, Bagatolli L A, Volovyk Z N, Thompson N L, Levi M, Jacobson K and Gratton E 2001 Lipid rafts reconstituted in model membranes *Biophys. J.* **80** 1417–28

[12] Dietrich C, Volovyk Z N, Levi M, Thompson N L and Jacobson K 2001 Partitioning of Thy-1, GM1, and cross-linked phospholipid analogs into lipid rafts reconstituted in supported model membrane monolayers *Proc. Natl Acad. Sci. USA* **98** 10642–7

[13] Dixon J F 2000 *Advances in Immunology* vol 75 (London: Academic)

[14] East L and Isacke C M 2002 The mannose receptor family *Biochim. Biophys. Acta* **1572** 364–86

[15] Eggens I, Fenderson B, Toyokuni T, Dean B, Stroud M and Hakomori S 1989 Specific interaction between lex and lex determinants—a possible basis for cell recognition in preimplantation embryos and in embryonal carcinoma-cells *J. Biol. Chem.* **264** 9476–84

[16] Fiani M L, Beitz J, Turvy D, Blum J S and Stahl P D 1998 Regulation of mannose receptor synthesis and turnover in mouse J774 macrophages *J. Leukocyte Biol.* **64** 85–91

[17] Gege C, Schneider M F, Schumacher G, Limozin L, Rothe U, Bendas G, Tanaka M and Schmidt R R 2004 Functional microdomains of glycolipids with partially fluorinated membrane anchors: impact on cell adhesion *Chemphyschem* **5** 216–24

[18] Hakomori S and Igarashi Y 1995 Functional-role of glycosphingolipids in cell recognition and signaling *J. Biochem.* **118** 1091–103

[19] Hillebrandt H and Tanaka M 2001 Electrochemical characterization of self-assembled alkylsiloxane monolayers on indium-tin oxide (ITO) semiconductor electrodes *J. Phys. Chem.* B **105** 4270–6

[20] Huang W J, Jin C Y, Derzon D K, Huber T A, Last J A, Provencio P P, Gopalan A S, Dugger M and Sasaki D Y 2004 Synthesis of ether-linked fluorocarbon surfactants and their aggregational properties in organic solvents *J. Colloid Interface Sci.* **272** 457–64

[21] Jacob G S, Kirmaier C, Abbas S Z, Howard S C, Steininger C N, Welply J K and Scudder P 1995 Binding of Sialyl-Lewis-X to E-selectin as measured by fluorescence polarization *Biochemistry* **34** 1210–7

[22] Jacobson K and Dietrich C 1999 Looking at lipid rafts? *Trends Cell Biol.* **9** 87–91

[23] Keller S L and McConnell H M 1999 Stripe phases in lipid monolayers near a miscibility critical point *Phys. Rev. Lett.* **82** 1602–5

[24] Krauss K and Altevogt P 1999 Integrin leukocyte function-associated antigen-1-mediated cell binding can be activated by clustering of membrane rafts *J. Biol. Chem.* **274** 36921–7

[25] Lipowsky R and Dimova R 2003 Domains in membranes and vesicles *J. Phys.: Condens. Matter* **15** S31–45

[26] Lowe J B and Ward P A 1997 Therapeutic inhibition of carbohydrate-protein interactions *in vivo J. Clin. Investig.* **99** 822–6

[27] McConnell H M 1991 Structures and transitions in lipid monolayers at the air–water-interface *Annu. Rev. Phys. Chem.* **42** 171–95

[28] Mori M, Ito Y and Ogawa T 1990 Total synthesis of the Mollu-series glycosyl ceramides—Alpha-D-Manp-(1-]3)-Beta-D-Manp-(1-]4)-Beta-D-Glcp-(1-]1)-Cer and Alpha-D-Manp-(1-]3)-[Beta-D-Xylp-(1-]2)]-Beta-D-Manp-(1-]4)-Beta-D-Glcp-(1-]1)-Cer *Carbohydr. Res.* **195** 199–224

[29] Oelke J, Pasc A, Wixforth A, Konovalov O and Tanaka M 2008 Highly uniform, strongly correlated fluorinated lipid nanodomains embedded in biological membrane models *Appl. Phys. Lett.* **93** 213901

[30] Quesada-Pérez M, Callejas-Fernández J and Hidalgo-Álvarez R 2002 Interaction potentials, structural ordering and effective charges in dispersions of charged colloidal particles *Adv. Colloid Interface Sci.* **95** 295–315

[31] Rosenberg R D, Shworak N W, Liu J, Schwartz J J and Zhang L J 1997 Heparan sulfate proteoglycans of the cardiovascular system. Specific structures emerge but how is synthesis regulated? *J. Clin. Investig.* **99** 2062–70
[32] Rothman J E and Lenard J 1977 Membrane asymmetry *Science* **195** 743–53
[33] Rowlinson J S 1969 *Liquids and Liquid Mixtures* (London: Butterworth)
[34] Russell S W 1992 *Macrophage Biology and Activation* vol 181 (Berlin: Springer)
[35] Schneider M F, Andelman D and Tanaka M 2005 Stripes of partially fluorinated alkyl chains: dipolar Langmuir monolayers *J. Chem. Phys.* **122** 094717
[36] Simons K and Ikonen E 1997 Functional rafts in cell membranes *Nature* **387** 569–72
[37] Thompson T E and Tillack T W 1985 Organization of glycosphingolipids in bilayers and plasma membranes of mammalian cells *Annu. Rev. Biophys. Biophys. Chem.* **14** 361–86
[38] Tristram-Nagle S, Petrache H I and Nagle J F 1998 Structure and interactions of fully hydrated dioleoylphosphatidylcholine bilayers *Biophys. J.* **75** 917–25
[39] Ushiyama S, Laue T M, Moore K L, Erickson H P and Mcever R P 1993 Structural and functional-characterization of monomeric soluble P-selectin and comparison with membrane P-selectin *J. Biol. Chem.* **268** 15229–37
[40] Varki A P, Kagnoff M F and Insel P A 1997 Passing the baton at high speed: time to hand over to a new editorial board *J. Clin. Investig.* **99** 553–4
[41] Verwey E J W and Overbeek J T G 1948 *Theory of the Stability of Lyophobic Colloids* (New York: Elsevier)
[42] Welply J K, Abbas S Z, Scudder P, Keene J L, Broschat K, Casnocha S, Gorka C, Steininger C, Howard S C, Schmuke J J, Graneto M, Rotsaert J M, Manger I D and Jacob G S 1994 Multivalent sialyl-lex—potent inhibitors of E-selectin-mediated cell-adhesion reagent for staining activated endothelial-cells *Glycobiology* **4** 259–65